J Appl Electrochem (2014) 44:105–113
DOI 10.1007/s10800-013-0606-6

RESEARCH ARTICLE

Carbon nanotubes/amorphous carbon composites as high-power negative electrodes in lithium ion capacitors

S. R. Sivakkumar · A. G. Pandolfo

Received: 18 June 2013 / Accepted: 5 August 2013 / Published online: 11 August 2013

Abstract A nitrogen-rich carbon nanotubes/amorphous carbon (CNT/C) composite was prepared by carbonising a CNT/polyaniline (PANI) composite, and characterised. Scanning electron microscopy and X-ray photoelectron spectroscopy confirmed that the composite retained a mesoporous CNT structure as its backbone, whilst the nitrogen-rich PANI-derived carbon formed a thin amorphous coating on the CNT surface. Electrochemical characterisation of the CNT/C composite indicated that it had nearly double the reversible Li^+ intercalation capacity (390 vs. 219 mAh g^{-1}) and 39 % less irreversible capacity (622 vs. 1,015 mAh g^{-1}) than the pristine CNT. The CNT/C composite showed exceptionally high rate capability with a de-intercalation capacity of 81 mAh g^{-1} at a very high charge/discharge rate of 60 C (time taken for charge or discharge is 1 min) (1 C = 1 h charge or discharge), whereas the pristine CNT delivered 53 mAh g^{-1} at this C-rate. By comparison, the rate capabilities of conventional graphite (N3 and SLP30) were very poor above 5 C ($\sim$17 mAh g^{-1} at 5 C). Both the pristine CNT and CNT/C composite showed an excellent cyclability at 1 C charge/discharge over 600 cycles. The CNT/C composite maintained a fairly stable capacity of $\sim$200 mAh g^{-1} after 600 cycles, whilst the commercial graphite showed a steady and significant decrease in de-intercalation capacity; reaching $<$70 mAh g^{-1} after 600 cycles.

S. R. Sivakkumar · A. G. Pandolfo
CSIRO Energy Technology, Box 312, Clayton South, VIC 3169, Australia

S. R. Sivakkumar (✉)
School of Chemical and Biotechnology, SASTRA University, Thanjavur 613 401, India
e-mail: srsivakkumar@scbt.sastra.edu

Keywords Lithium ion capacitor · Supercapacitor · Lithium ion battery · Anode · CNT

1 Introduction

Lithium ion capacitors (LICs) are advanced hybrid energy-storage devices capable of storing 5–10 times more energy than conventional electric double layer capacitors and have similar levels of high power and long cycle life [1–13]. LICs are typically assembled with a lithium ion intercalating anode and a high-surface–area-activated carbon (AC) cathode, together with a carbonate-based electrolyte-containing $LiPF_6$. During the charge/discharge of an LIC, lithium ions intercalate/de-intercalate at the negative electrode, whereas depending upon the cell cut-off voltage, either PF_6^- or Li^+ adsorb/desorb at the positive electrode. As the lithium intercalation/de-intercalation process occurring at the negative electrode is a relatively slow process (compared with the fast ion adsorption/desorption process occurring at the positive electrode), the rate capability of a LIC is generally limited by the negative electrode kinetics.

Among various Li^+ intercalating negative electrode materials, graphitic carbons are frequently used as they have many benefits including a low Li intercalation potential (0.1–0.2 V vs. Li/Li^+), high capacity, a flat charge/discharge voltage profile, high cycling and thermal stability, safety and relatively low cost. A recent report demonstrates that whilst commercial graphite materials generally have good de-intercalation capabilities, their Li^+ intercalation rate capability is relatively poor [14]. Therefore, when graphite is used as a negative electrode in a LIC, the device will suffer from slow charge rate limitations; as is regularly observed with many lithium-ion batteries (LIBs) that also use a graphite anode. Since LIC is a power

device, it will be required to charge at a very fast rate, and therefore, classical graphite is unlikely to be a suitable negative electrode material.

A review of the literature reveals that several forms of carbon-based materials have been trialled as negative electrodes in LICs and LIBs and can be broadly categorised into: AC/pitch-based composites [3], disordered carbon [4, 15–27], non-graphitisable carbon [5], bimodal/hierarchical porous carbon [6, 28–36], graphite/composites [7, 8, 37–45], polyacene [12] and mesoporous carbon [13].

Carbon materials prepared at temperatures below 1,000 °C tend to be predominantly amorphous in structure with a low degree of graphitisation. These amorphous materials usually show an improved Li intercalation/de-intercalation rate capability, but the Li de-insertion voltage profiles show a monotonous change of voltage during discharge and appear to behave more like capacitive materials (i.e. a linear change of voltage with charge/discharge; unlike the flat charge/discharge profile obtained with graphite). They also tend to display a high irreversible capacity due to the presence of a large number of micropores. When carbonisation temperatures above ~2,000 °C are employed, the carbons begin to graphitise (increase in graphene ring size and number of stacking layers) and begin to behave in a similar way to classical graphite, i.e., high capacity but poor charge rate. Composite carbon materials with an amorphous carbon coating (shell) on the surface of graphite (core) have also been prepared with a decreased irreversible capacity and improved chemical and physical stability [37–45]; however, as the active core is still highly graphitic, the rate capability was not observed to increase appreciably.

Another approach has been the preparation of carbons with a hierarchical pore structure containing a 3D network of interconnecting pores of varying size ranges. In this approach, hard and soft templates have been employed whereby a carbon precursor is impregnated into a silica template and carbonised before the template is removed by HF etching [28–36]. Whilst the carbons have hierarchical 3D network of pores, upon subsequent high temperature treatment (above 2,000 °C) and further graphitisation, the material tends to behave in a similar manner to classical graphite. It appears that in addition to porosity, a limited or controlled graphitisation of carbons may be required to achieve a high rate capability. A reduced level of graphitisation would reduce the intercalation capacity of the carbon; however, as capacity of a LIC will be limited by the positive AC electrode, a decrease in the capacity of the negative intercalation electrode may not be detrimental.

The appropriate selection of electrolyte and electrode porosity will be the key factors controlling the rate capability of graphitic carbon electrodes [46]. Carbons having a mesoporous, 3D network and less-graphitic structure are presumed to be more promising materials to achieve a high charge rate capability. The carbon nanotube (CNT) materials fulfil these characteristics, and numerous publications studying the electrochemical performance of CNTs are available in the literature [47–64]. A vertically aligned multi-wall CNT electrode was shown to have a reversible capacity of 166 mAh g^{-1} @ 70 C rate (charge or discharge time: 51 s) [60], whilst a similar capacity was reported for unaligned multi-wall CNT electrodes operating at 10 C (charge or discharge time: 6 min) [54]. Specific capacities of multi-walled CNTs are reported to be in the range of 100–600 mAh g^{-1}, depending on the preparation method; however a high irreversible capacity, low volumetric density and poor voltage profile during discharge limit their application as electrode materials in LIBs [53].

There has also been interest in improving the specific capacity and rate of CNTs by nitrogen doping [53]. Towards this end, we have characterised a CNT/C composite, prepared by carbonising polyaniline (PANI) onto CNT to form a nitrogen-rich CNT/amorphous carbon (C) composite. To our knowledge, a performance evaluation of this type of composite material has not been reported earlier, especially in the context of its use in high-power LICs. In the present study, the CNT/C composite is characterised and its electrochemical Li^+ storage properties are evaluated and compared with conventional graphite.

2 Experimental

Multi-walled CNTs (prepared by chemical vapour deposition) were purchased from Iljin Nanotech, Korea. Commercial graphites prescribed for high-power LIB anode, N3 (ConocoPhillips; D_{50}, 3 μm) and SLP30 (Timcal; D_{50}, 30 μm) were obtained from the suppliers. All other chemicals were purchased from Aldrich.

The composite was prepared by in situ polymerisation following a previously reported procedure [63]; except, HCl was used in place of $HClO_4$. The freshly prepared CNT/PANI composite was estimated to have 30 wt% of CNT and 70 wt% of PANI. Samples of the dry composite were pre-weighed into a crucible prior to carbonisation at various temperatures: 600, 700, 800 and 900 °C under a flowing N_2 atmosphere. The heating rate was 2.5 °C/min from room temperature and held at the final temperature for 1 h before overnight cooling under flowing N_2. The carbonised composite (CNT/C) was then reweighed to determine the ratio of CNT to the carbon derived from PANI. The composite was gently milled (FRITSCH pulverisette 6) at 300 rpm for 10 min to produce a fine powder suitable for the preparation of electrodes by slurry coating. For comparison, pristine CNT was also heat-treated using the same protocol.

Scanning electron micrographs (SEM) of CNT and its composite powders were obtained using a Philips XL30 FESEM. Brunauer–Emmett–Teller (BET) surface area of CNT-based materials was measured using a Micromeritics ASAP 2400 gas sorption analyser. Powder X-ray diffraction profiles were collected using a Philips X'Pert MPD (PW 1800) diffractometer equipped with a copper target X-ray tube. X-ray photoelectron spectra (XPS) were acquired using a high-resolution Kratos XPS instrument.

Carbon electrodes were prepared by coating a mixture of the carbon sample (1.0 g), a conductive carbon black (Super P–Li, 0.06 g) and carboxymethyl cellulose salt binder (0.1 g) dispersed in water, onto 100-μm-thick copper mesh (dimension: 2 cm × 2 cm) (one of the sides masked by a polyimide tap) using a grooved-rod applicator at a thickness of 60 μm. All the coated electrodes were roll-pressed and dried at 100 °C overnight under dynamic vacuum before testing. Pristine CNT electrodes were prepared in a similar fashion as above but without a conductive carbon black. The coated electrodes were cut into electrodes with an active area of: 2 cm × 2 cm and a 3 cm tab. Li metal (250 μm thick, Aldrich) electrodes of dimension 2 cm × 2 cm were prepared by roll-pressing Li onto a copper foil with a 3 cm tab. Two electrode cells comprising carbon and Li electrodes were assembled in metallised plastic packaging (i.e. pouch cells) by sandwiching the electrodes on either side of a polyolefin (Solupor) separator (38 μm thick). The pouch cells were hermetically sealed after the addition of electrolyte (ethylene carbonate/dimethyl carbonate mixture (50:50 w/w) containing 1 M $LiPF_6$ salt (Sol-Rite, Mitsubishi Chemical Corp., Japan)). All cells were assembled in an Argon-filled glove box. Galvanostatic charge/discharge cycling of the cells was performed using a Maccor (Series 4000) battery cycler. No constant voltage float was applied when the cell voltages reached the cut-off voltages (0.005–2.0 V vs. Li/Li^+), but a rest period of 30 s was applied. Specific capacity values are calculated based on the combined masses of the active material and the carbon black (combined masses were in the range of 2–3 mg cm^{-2}) (mass of the binder was not considered). All electrochemical tests were performed at ambient temperature.

3 Results and discussion

The pristine CNT sample exhibited no weight loss after heat treatments up to 900 °C. Therefore, it was considered that the absolute weight of CNT in the CNT/PANI composites did not change during carbonisation. Accordingly, the weight percentage of CNT in the composites was determined to be: 75.1, 70.5, 65.2 and 67.3 % and, by difference, the proportion of carbon derived from PANI was: 24.8, 29.4, 34.7 and 32.6 % by weight for the samples heat-treated at 600, 700, 800 and 900 °C, respectively. These weight measurements confirm the presence of a significant amount PANI-derived material in the composite after carbonisation.

The BET surface area and pore size of the pristine CNT and the composite carbonised at various temperatures are presented in Table 1. The pristine CNT has a predominantly mesoporous structure, with a BET surface area of ~222 m^2/g. Both the surface area and pore volumes decrease significantly after carbonisation, which is attributed to a pore size reduction resulting from a surface coverage and partial infiltration of the PANI-derived carbon into the CNT mesostructure.

Figure 1 displays the XRD patterns of the: CNT, PANI and CNT/PANI heat-treated at 800 °C (CNT/C) samples, and the corresponding peak positions and d-spacing values calculated for these samples are presented in Table 2. The CNT displays a typical (002) peak at 25.98° corresponding to a graphite-like structure. The PANI-derived carbon (PANI-800) displays a very broad peak typical of materials with poor crystallinity, whilst the CNT/C composite also displays a peak similar to the CNT, but with a lower peak intensity. This (002) peak intensity is seen to increase with increase in carbonisation temperature (inset in Fig. 1), indicating an increase in degree of graphitisation with increase in temperature [32, 45].

In order to further establish the presence of amorphous carbon coating in the composite, and to identify its chemical composition, XPS was recorded for the CNT/C composite prepared at 800 °C. The spectra obtained along with other samples for comparison are presented in Fig. 2 and the XPS-derived chemical composition of these samples is given in Table 3. The C1*s* spectra for all the samples show a single peak with the samples containing PANI or PANI-derived carbon exhibiting significant peak broadening. The N1*s* spectrum confirms the presence of nitrogen in the composite samples (note the absence of nitrogen signal from pristine and heat-treated CNTs). The nitrogen signal at 399–399.5 eV from the CNT/PANI composite is attributed to the presence of PANI. After heat-treating the composite, the original nitrogen peak disappears and two new N1*s* peaks appear at 398 eV and 400.5–401 eV in the carbonised sample, which are attributed to pyridinic nitrogen and to pyrrolic nitrogen (and/or quaternary nitrogen), respectively [64–67]. The XPS data confirms the chemical incorporation of PANI-derived (but modified) nitrogen structures in the heat-treated CNT/C composite, and Table 3 shows that the 800 °C heat-treated composite contains as much as 6.7 % of nitrogen by atomic concentration.

Scanning electron micrograph images of the pristine CNT and the heat-treated CNT/C composites are presented

Table 1 Physical properties of pristine CNT and CNT/C composites

Sample	BET area (m^2 g^{-1})	Vt[a] (cm^3 g^{-1})	Average pore diameter (nm)	Vmic[b] (cm^3 g^{-1})	Vmeso[c] (cm^3 g^{-1})
Pristine CNT	222	1.03	16.00	0.08	0.95
CNT/C-600	225	0.38	4.84	0.09	0.29
CNT/C-700	215	0.36	12.00	0.09	0.27
CNT/C-800	181	0.44	15.32	0.07	0.37
CNT/C-900	171	0.40	14.00	0.07	0.33

[a] Total volume

[b] Microporous volume

[c] Mesoporous volume

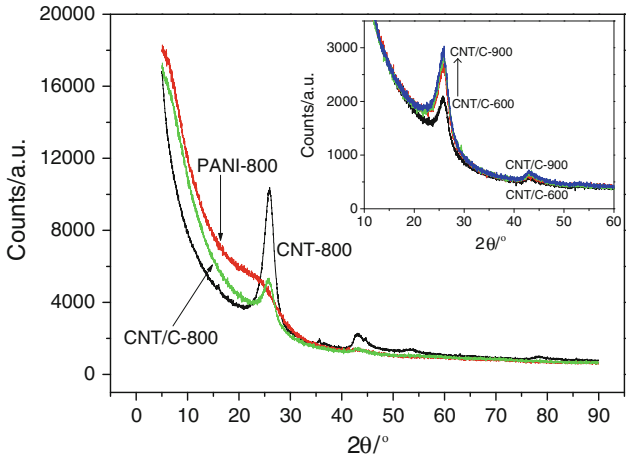

Fig. 1 XRD patterns of CNT, PANI and CNT/C heat-treated at 800 °C. *Inset* CNT/C composite obtained by heat-treating at various temperatures such as 600, 700, 800 and 900 °C

Table 2 XRD results of samples heat-treated at 800 °C

Sample	Peak 1		Peak 2	
	Degree	*d*-spacing (nm)	Degree	*d*-spacing (nm)
CNT-800	25.981	0.3425	42.934	0.2100
PANI-800	24.146 (broad)	0.3676	42.980	0.2103
CNT/C-800	25.841	0.3443	42.743	0.2113

in Fig. 3. The images of composites show that the CNTs are intimately covered with the PANI-derived carbon material but, the composite still maintains an open network structure. As the carbonisation temperature increases, the increased burn-off of the PANI results in a more open arrangement with the CNT support structure becoming more visible in the composite carbonised at 900 °C.

The initial experiments on evaluating the electrochemical performance of the CNT/C composites obtained at various carbonising temperatures showed that the material carbonised at 800 °C displayed the best performance and therefore the electrochemical performance for only the composite carbonised at 800 °C is discussed hereinafter.

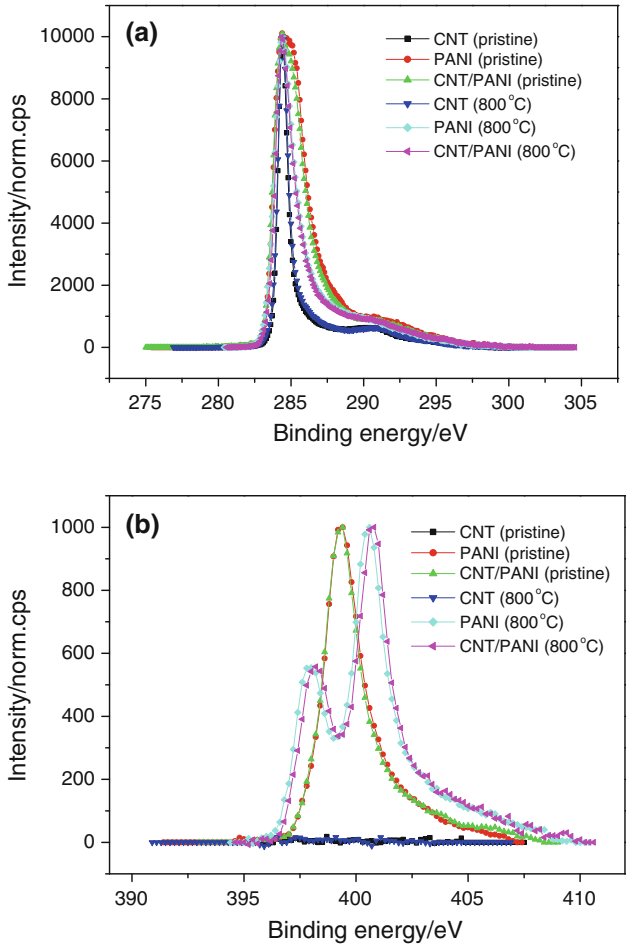

Fig. 2 XPS spectra of **a** C1*s* and **b** N1*s* of samples

The galvanostatic charge/discharge curves obtained from the CNT/C composite and the pristine CNT (versus Li counter electrode) are shown in Fig. 4. The CNT/C composite displayed a charge capacity of 1,012 mAh g^{-1} and discharge capacity of 390 mAh g^{-1} (irreversible capacity: 622 mAh g^{-1}), whereas the pristine CNT displayed a charge capacity of 1,234 mAh g^{-1} and discharge capacity of 219 mAh g^{-1} (irreversible capacity: 1,015 mAh g^{-1}). The CNT/C composite has a greater reversible capacity (nearly double) and less irreversible capacity (39 % less)

Table 3 Chemical composition of samples: atomic concentrations are relative to the total concentration of C (atomic ratios X/C)

Element	Pristine CNT	CNT-800	Pristine PANI	PANI-800	Pristine CNT/PANI	CNT/PANI-800
C	1.0000	1.0000	1.0000	1.0000	1.0000	1.0000
O	0.0086	0.0064	0.0607	0.0225	0.0598	0.0204
N	0.0021	0.0009	0.1756	0.0786	0.1633	0.0670

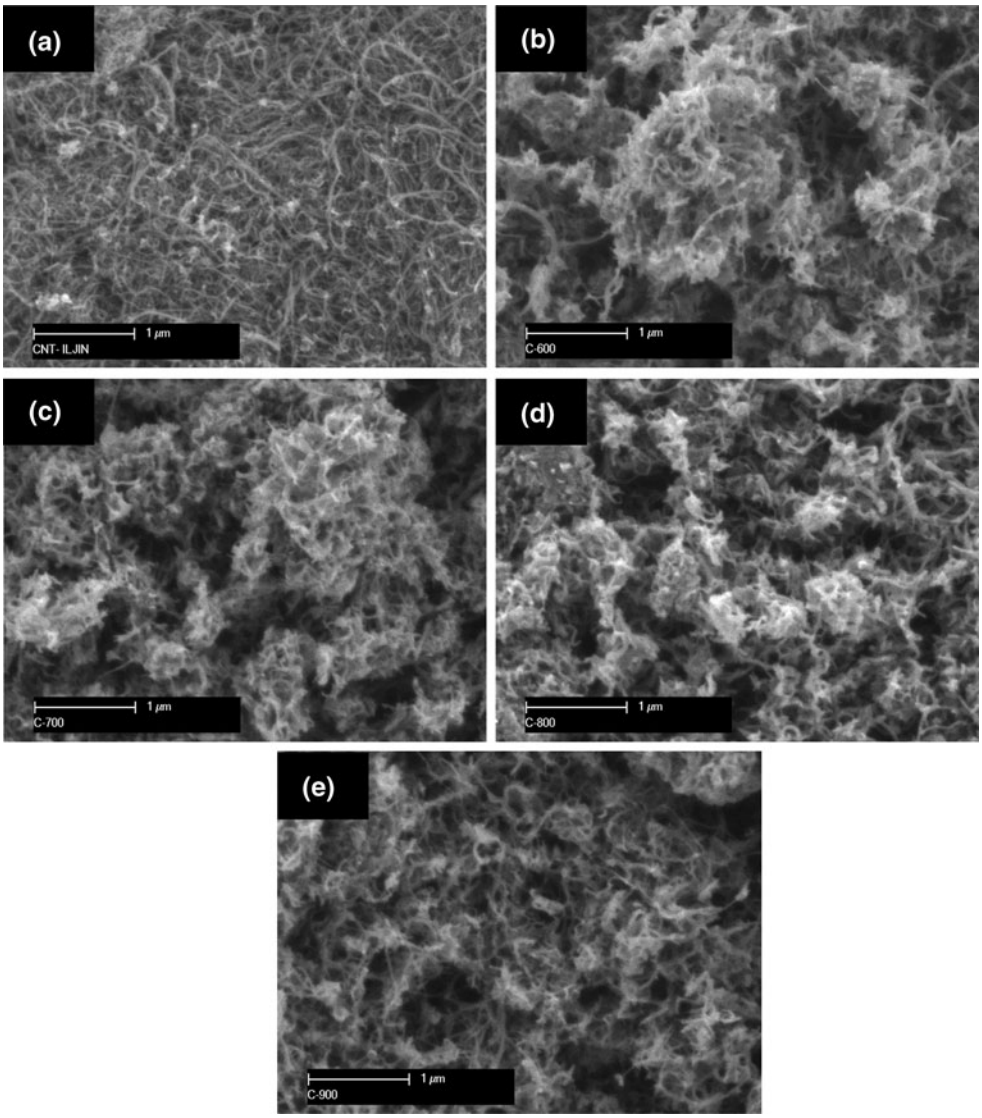

Fig. 3 SEM images of **a** pristine CNT and CNT/C composite obtained by heat-treating at **b** 600 °C, **c** 700 °C, **d** 800 °C and **e** 900 °C

compared with the pristine CNT. A plateau observed at 0.9 V during charging the pristine CNT electrode is reported to be due the formation of a solid electrolyte interface (SEI) layer [53], and such a plateau is not observed with the CNT/C composite, indicating the SEI layer formation mechanisms are different for these two materials.

The rather curved charge/discharge profiles observed in Fig. 4, and the relatively high BET surface area of the composite suggest that, in addition to Li^+ intercalation, the Li^+ charge storage mechanism may also involve Li^+ adsorption. The greater reversible capacity of the CNT/C composite over pristine CNT is believed to be due to the presence of nitrogen (derived from PANI) in the composite. It has been well recognised that the nitrogen doping in carbon materials increases the charge storage capacity of electrochemical materials [64–70]. In those studies, the increased capacity was attributed to (i) the presence of nitrogen improving the wettability of the electrode material

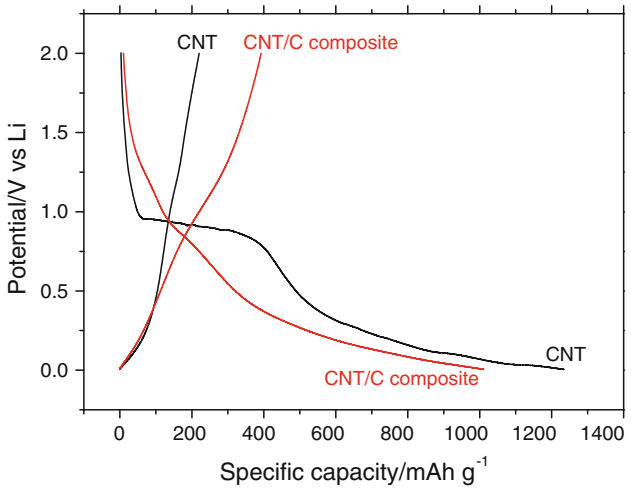

Fig. 4 Charge/discharge curves of pristine *CNT* and *CNT/C* composite obtained during the first cycle. Current rate: C/40

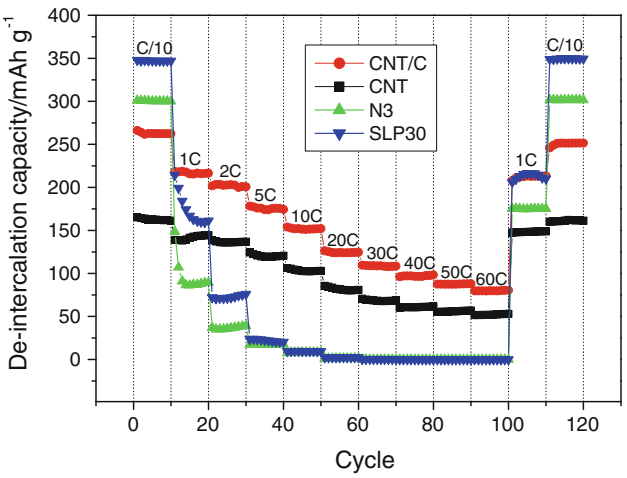

Fig. 5 Comparison of rate capability of CNT/C composite with pristine CNT and two other commercial graphite materials. Intercalation rate was 'same' as that of de-intercalation rate

(with the electrolyte), resulting in a greater accessible surface area and (ii) nitrogen-containing ring structures/functionalities that can undergo faradaic redox reactions, thereby contributing additional charge storage capacity.

In order to determine the suitability of CNT/C composite for use as high-power negative electrodes, the rate capabilities of the composite were evaluated at up to 60 C (1 min charge/discharge) and the results compared with pristine CNT and two other LIB-grade commercial graphites, N3 and SLP-30 (Fig. 5). In these trials, the current rate equivalent to 1 C is taken as 372 mA/g for all the materials (theoretical capacity of graphite: 372 mAh g^{-1}). It should also be highlighted that the intercalation rate was the 'same' as that of de-intercalation rate (for example: for the de-intercalation rate of 60 C, the intercalation rate was also 60 C). All the cells were conditioned by cycling at C/40 rate for three cycles and their capacity was recorded for consecutive 10 cycles at each C-rate.

Both the commercial graphites (N3 and SLP30) have a similar behaviour displaying very high capacities at C/10 (305 and 345 mAh g^{-1}, respectively), but their capacities decrease rapidly as the C-rate increases (even at 1 C) and both graphites show almost negligible capacity above 5 C. The pristine CNT sample has a modest initial capacity at C/10 ($\sim$170 mAh g^{-1}), but its performance at higher rates (2 C and above) is superior to that of the commercial graphites, and it also displays a very creditable 53 mAh g^{-1} at the extremely high rate of 60 C. In comparison, the CNT/C composite material has an initial C/10 capacity of 265 mAh g^{-1}. The higher capacity of the CNT/C composite, over pristine CNT sample, can be attributed to the presence of the nitrogen-containing amorphous carbon coating as discussed previously. In addition, the intrinsic high rate capability of the CNT is maintained in the CNT/C composite with 81 mAh g^{-1} deliverable at 60 C. After 100 cycles of testing at various C-rates, the cells were recycled at 1 C and C/10 during which all cells recovered their initial capacity (Fig. 5). This not only confirms the stability of the cells but also establishes that the low capacity values obtained at high C-rates were not due to electrode material degradation but rather were limited by the respective electrode kinetics. This is consistent with a recent study that has demonstrated that whilst commercial graphites have good de-intercalation rates, their intercalation rate capability is relatively poor [14].

The cycle life performance of the CNT/C composite, pristine CNT, N3 and SLP30 was evaluated at the reasonably fast charge/discharge rate of 1 C and the results are presented in Fig. 6. The pristine CNT (Fig. 6a) shows excellent stability during over 600 cycles. The CNT/C composite shows a small drop in capacity during the initial 50 cycles, but, thereafter, it maintains fairly stable capacity on cycling. Again, the greater reversible capacity of the CNT/C composite compared with the pristine CNT is very significant. In contrast, the N3 and SLP30 shows a steady decrease in capacity on cycling (at this C-rate). The cyclability of both these materials is found to be very similar; however, after 600 cycles, the reversible capacities of these materials are below $\sim$70 mAh g^{-1}. After cycling, the graphite samples were reconditioned and recycled at both C/10 and 1 C rates for 10 cycles (data not shown). Whilst some small recovery in reversible capacity was observed, their capacities continued to decrease indicting that the N3 and SLP30 graphites have undergone some irreversible degradation after cycling.

4 Conclusions

A nitrogen-rich CNT/C composite is prepared by carbonising a CNT/PANI composite. The mesoporous tubular

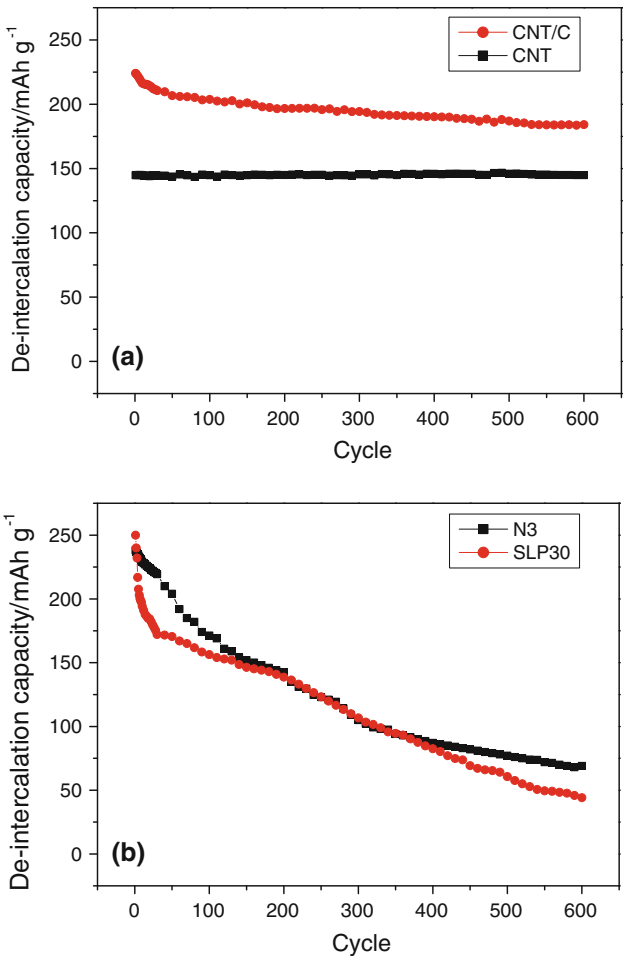

Fig. 6 Cycle life behaviour of **a** CNT/C composite and pristine CNT and **b** two commercial graphites. Charge/discharge rate: 1 C

architecture of the CNT, its relatively higher graphene interlayer distance (0.342 vs. 0.335 nm for graphite) and the nature of charge storage mechanism appear to play a crucial role in realising high-rate capability (especially intercalation rate) of CNT-based electrodes in comparison with conventional graphite.

Electrochemical characterisation of the CNT/C composite in comparison with the pristine CNT material indicate that the composite has nearly double the reversible capacity (390 vs. 219 mAh g^{-1}) and 39 % less irreversible capacity (622 vs. 1,015 mAh g^{-1}) during the first cycle at C/40 rate. For the same coating thickness, the loading of CNT/C composite weighs at least twice in comparison with the pristine CNT, which is another benefit of the CNT/C composite to obtain higher volumetric capacity. The CNT/C composite shows exceptionally high rate capability with a de-intercalation capacity of 81 mAh g^{-1} at a very high charge/discharge rate of 60 C; whereas, the pristine CNT delivers 53 mAh g^{-1} at this C-rate. The rate capabilities of conventional graphites (N3 and SLP30) are very poor beyond 5 C ($\leq$17 mAh g^{-1} at 5 C).

Cycle life testing at 1 C charge/discharge rate shows an excellent cyclability of pristine CNT delivering a capacity of 146 mAh g^{-1} with no capacity degradation after 600 cycles. The CNT/C composite shows a small drop in capacity during the initial 50 cycles; thereafter, it maintains a fairly stable capacity of $\sim$200 mAh g^{-1} for up to 600 cycles. The commercial graphites show a steady and significant decrease in de-intercalation capacity from the initial value of 239 mAh g^{-1} for N3 and 250 mAh g^{-1} for SLP30 to 69 mAh g^{-1} for N3 and 44 mAh g^{-1} for SLP30 after 600 cycles.

As the negative electrodes in LICs are generally predoped with metallic lithium [3, 5, 7, 12, 13] (to improve the cycle life and energy density of the device), the relatively high irreversible capacity of the CNT/C composite during the first cycle should not limit its use in LIC, and therefore, it is concluded that the CNT/C composite is a promising negative electrode material for high-power LICs.

Acknowledgments This work was made possible by funding through the CSIRO Energy Transformed Flagship. The assistance of Dr. Vanesa Ruiz with BET surface area measurement and Dr. Thomas Gengenbach (CSIRO) with XPS analysis is also gratefully acknowledged.

References

1. Amatucci GG, Badway F, Pasquier AD, Zheng T (2001) An asymmetric hybrid nonaqueous energy storage cell. J Electrochem Soc 148:A930–A939. doi:10.1149/1.1383553
2. Pasquier AD, Plitz I, Menocal S, Amatucci G (2003) A comparative study of Li-ion battery, supercapacitor and nonaqueous asymmetric hybrid devices for automotive applications. J Power Sources 115:171–178. doi:10.1016/S0378-7753(02)00718-8
3. Yoshino A, Tsubata T, Shimoyamada M, Satake H, Okano Y, Mori S, Yata S (2004) Development of a lithium-type advanced energy storage device. J Electrochem Soc 151:A2180–A2182. doi:10.1149/1.1813671
4. Ogihara N, Igarashi Y, Kamakura A, Naoi K, Kusachi Y, Utsugi K (2006) Disordered carbon negative electrode for electrochemical capacitors and high-rate batteries. Electrochim Acta 52:1713–1720. doi:10.1016/j.electacta.2006.01.082
5. Aida T, Murayama I, Yamada K, Morita M (2007) Analyses of capacity loss and improvement of cycle performance for a high-voltage hybrid electrochemical capacitor. J Electrochem Soc 154:A798–A804. doi:10.1149/1.2746562
6. Woo SW, Dokko K, Nakano H, Kanamura K (2007) Bimodal porous carbon as a negative electrode material for lithium-ion capacitors. Electrochemistry 75:635–640. doi:10.5796/electrochemistry.75.635
7. Aida T, Murayama I, Yamada K, Morita M (2007) Improvement in cycle performance of a high-voltage hybrid electrochemical capacitor. Electrochem Solid State Lett 10:A93–A96. doi:10.1149/1.2435511
8. Khomenko V, Pinero ER, Beguin F (2008) High-energy density graphite/AC capacitor in organic electrolyte. J Power Sources 177:643–651. doi:10.1016/j.jpowsour.2007.11.101
9. Wu F, Lu H, Su Y, Chen S, Guan Y (2010) A simple way of predoping lithium ion into carbon negative electrode for lithium ion capacitor. Mater Sci Forum 650:142–149. doi:10.4028/www.scientific.net/MSF.650.142

10. Naoi K, Simon P (2008) New materials and new configurations for advanced electrochemical capacitors. Electrochem Soc Interface 17:34–37
11. Karthikeyan K, Aravindan V, Lee SB, Jang IC, Lim HH, Park GJ, Yoshio M, Lee YS (2010) A novel asymmetric hybrid supercapacitor based on Li_2FeSiO_4 and activated carbon electrodes. J Alloys Compd 504:224–227. doi:10.1016/j.jallcom.2010.05.097
12. Aida T, Yamada K, Morita M (2006) An advanced hybrid electrochemical capacitor that uses a wide potential range at the positive electrode. Electrochem Solid State Lett 9:A534–A536. doi:10.1149/1.2349495
13. Hatozaki O (2008) Improvement of lithium ion capacitor with new electrode materials. In: Proceedings of the 18th international seminar on double layer capacitors and hybrid energy storage devices, 8–10 December. Deerfield beach, Florida, USA, pp 96–112
14. Sivakkumar SR, Nerkar JY, Pandolfo AG (2010) Rate capability of graphite materials as negative electrodes in lithium-ion capacitors. Electrochim Acta 55:3330–3335. doi:10.1016/j.electacta.2010.01.059
15. Takami N, Satoh A, Hara M, Ohsaki T (1995) Rechargeable lithium-ion cells using graphitized mesophase-pitch-based carbon fiber anodes. J Electrochem Soc 142:2564–2571. doi:10.1149/1.2050054
16. Ohsaki T, Kanda M, Aoki Y, Shiroki H, Suzuki S (1997) High-capacity lithium-ion cells using graphitized mesophase-pitch-based carbon fiber anodes. J Power Sources 68:102–105. doi:10.1016/S0378-7753(97)02634-7
17. Mochida I, Ku CH, Yoon SH, Korai Y (1998) Anodic performance and mechanism of mesophase-pitch-derived carbons in lithium ion batteries. J Power Sources 75:214–222. doi:10.1016/S0378-7753(98)00101-3
18. Suzuki K, Iijima T, Wakihara M (1999) Electrode characteristics of pitch-based carbon fiber as an anode in lithium rechargeable battery. Electrochim Acta 44:2185–2191. doi:10.1016/S0013-4686(98)00345-4
19. Tamai H, Sugahara H, Yasuda H (2000) Preparation of carbons from pitch containing polysilane and their anode properties for lithium-ion batteries. J Mater Sci Lett 19:53–56. doi:10.1023/A:1006703931974
20. Yang KS, Yoon YJ, Lee MS, Lee WJ, Kim JH (2002) Further carbonization of anisotropic and isotropic pitch-based carbons by microwave irradiation. Carbon 40:897–903. doi:10.1016/S0008-6223(01)00210-X
21. Lu W, Chung DDL (2003) Effect of the pitch-based carbon anode on the capacity loss of lithium-ion secondary battery. Carbon 41:945–950. doi:10.1016/S0008-6223(02)00435-9
22. Fey GTK, Lee DC, Lin YY (2003) High-capacity carbons prepared from acrylonitrile–butadiene–styrene terpolymer for use as an anode material in lithium-ion batteries. J Power Sources 119–121:39–44. doi:10.1016/S0378-7753(03)00121-6
23. Park SH, Kim C, Jeong YI, Lim DY, Lee YE, Yang KS (2004) Activation behaviors of isotropic pitch-based carbon fibers from electrospinning and melt spinning. Synth Met 146:207–212. doi:10.1016/j.synthmet.2004.07.004
24. Yi Z, Liang Y, Lei X, Wang C, Sun J (2007) Low-temperature synthesis of nanosized disordered carbon spheres as an anode material for lithium ion batteries. Mater Lett 61:4199–4203. doi:10.1016/j.matlet.2007.01.054
25. Hwang YJ, Jeong SK, Nahm KS, Shin JS, Stephan AM (2007) Pyrolytic carbon derived from coffee shells as anode materials for lithium batteries. J Phys Chem Solids 68:182–188. doi:10.1016/j.jpcs.2006.10.007
26. Zhang F, Ma H, Chen J, Li GD, Zhang Y, Chen JS (2008) Preparation and gas storage of high surface area microporous carbon derived from biomass source cornstalks. Bioresour Technol 99:4803–4808. doi:10.1016/j.biortech.2007.09.052
27. Zhang F, Wang KX, Li GD, Chen JS (2009) Hierarchical porous carbon derived from rice straw for lithium ion batteries with high-rate performance. Electrochem Commun 11:130–133. doi:10.1016/j.elecom.2008.10.041
28. Pang J, Hu Q, Wu Z, Hampsey JE, He J, Lu Y (2004) Direct synthesis of unimodal and bimodal nanoporous carbon. Microporous and Mesoporous Mater 74:73–78. doi:10.1016/j.micromeso.2004.06.009
29. Kwon OJ, Jung YS, Kim JH, Oh SM (2004) A simple preparation method for spherical carbons and their anodic performance in lithium secondary batteries. J Power Sources 125:221–227. doi:10.1016/j.jpowsour.2003.08.012
30. Wang T, Liu X, Zhao D, Jiang Z (2004) The unusual electrochemical characteristics of a novel three-dimensional ordered bicontinuous mesoporous carbon. Chem Phys Lett 389:327–331. doi:10.1016/j.cplett.2004.03.086
31. Yoon SB, Chai GS, Kang SK, Yu JS, Gierszal KP, Jaroniec M (2005) Graphitized pitch-based carbons with ordered nanopores synthesized by using colloidal crystals as templates. J Am Chem Soc 127:4188–4189. doi:10.1021/ja0423466
32. Hu YS, Adelhelm P, Smarsly BM, Hore S, Antonietti M, Maier J (2007) Synthesis of hierarchically porous carbon monoliths with highly ordered microstructure and their application in rechargeable lithium batteries with high-rate capability. Adv Funct Mater 17:1873–1878. doi:10.1002/adfm.200601152
33. Wang DW, Li F, Liu M, Lu GQ, Cheng HM (2008) 3D Aperiodic hierarchical porous graphitic carbon material for high-rate electrochemical capacitive energy storage. Angew Chem Int Ed 47:373–376. doi:10.1002/anie.200702721
34. Yamada H, Watanabe Y, Moriguchi I, Kudo T (2008) Rate capability of lithium intercalation into nano-porous graphitized carbons. Solid State Ionics 179:1706–1709. doi:10.1016/j.ssi.2008.02.022
35. Lee KT, Ji X, Rault M, Nazar LF (2009) Simple synthesis of graphitic ordered mesoporous carbon materials by a solid-state method using metal phthalocyanines. Angew Chem 121:5771–5775. doi:10.1002/ange.200806208
36. Li S, Liang Y, Wu D, Fu R (2010) Fabrication of bimodal mesoporous carbons from petroleum pitch by a one-step nanocasting method. Carbon 48:839–843. doi:10.1016/j.carbon.2009.10.037
37. Lee HY, Baek JK, Jang SW, Lee SM, Hong ST, Lee KY, Kim MH (2001) Characteristics of carbon-coated graphite prepared from mixture of graphite and polyvinylchloride as anode materials for lithium ion batteries. J Power Sources 101:206–212. doi:10.1016/S0378-7753(01)00671-1
38. Baek K, Lee HY, Jang SW, Lee SM (2005) Electrochemical performance of modified synthetic graphite for lithium ion batteries. J Mater Sci 40:347–353. doi:10.1007/s10853-005-6089-z
39. Guoping W, Bolan Z, Min Y, Xiaoluo X, Meizheng Q, Zuolong Y (2005) A modified graphite anode with high initial efficiency and excellent cycle life expectation. Solid State Ionics 176:905–909. doi:10.1016/j.ssi.2004.11.009
40. Lee JH, Lee HY, Oh SM, Lee SJ, Lee KY, Lee SM (2007) Effect of carbon coating on electrochemical performance of hard carbons as anode materials for lithium-ion batteries. J Power Sources 166:250–254. doi:10.1016/j.jpowsour.2006.12.078
41. Imanishi N, Ono Y, Hanai K, Uchiyama R, Liu Y, Hirano A, Takeda Y, Yamamoto O (2008) Surface-modified meso-carbon microbeads anode for dry polymer lithium-ion batteries. J Power Sources 178:744–750. doi:10.1016/j.jpowsour.2007.09.035
42. Zhang HL, Li F, Liu C, Cheng HM (2008) Poly(vinyl chloride) (PVC) coated idea revisited: influence of carbonization procedures on PVC-coated natural graphite as anode materials for lithium ion batteries. J Phys Chem C 112:7767–7772. doi:10.1021/jp8003536

43. Ohta N, Nagaoka K, Hoshi K, Bitoh S, Inagaki M (2009) Carbon-coated graphite for anode of lithium ion rechargeable batteries: graphite substrates for carbon coating. J Power Sources 194: 985–990. doi:10.1016/j.jpowsour.2009.06.013
44. Nozaki H, Nagaoka K, Hoshi K, Ohta N, Inagaki M (2009) Carbon-coated graphite for anode of lithium ion rechargeable batteries: carbon coating conditions and precursors. J Power Sources 194:486–493. doi:10.1016/j.jpowsour.2009.05.040
45. Park DY, Park DY, Lan Y, Lim YS, Kim MS (2009) High rate capability of carbonaceous composites as anode electrodes for lithium-ion secondary battery. J Ind Eng Chem 15:588–594. doi:10.1016/j.jiec.2009.03.001
46. Sawai K, Ohzuku T (2003) Factors affecting rate capability of graphite electrodes for lithium-ion batteries. J Electrochem Soc 150:A674–A678. doi:10.1149/1.1568107
47. Chen WX, Lee JY, Liu Z (2002) Electrochemical lithiation and de-lithiation of carbon nanotube–Sn_2Sb nanocomposites. Electrochem Commun 4:260–265. doi:10.1016/S1388-2481(02)00268-0
48. Shin HC, Liu M, Sadanadan B, Rao AM (2004) Lithium insertion into chemically etched multi-walled carbon nanotubes. J Solid State Electrochem 8:908–913. doi:10.1007/s10008-004-0498-9
49. Ng SH, Wang J, Guo ZP, Chen J, Wang GX, Liu HK (2005) Single wall carbon nanotube paper as anode for lithium-ion battery. Electrochim Acta 51:23–28. doi:10.1016/j.electacta.2005.04.045
50. Moriguchi I, Hidaka R, Yamada H, Kudo T, Murakami H, Nakashima N (2006) A mesoporous nanocomposite of TiO_2 and carbon nanotubes as a high-rate Li-intercalation electrode material. Adv Mater 18:69–73. doi:10.1002/adma.200501366
51. Lin K, Xu Y, He G, Wang X (2006) The kinetic and thermodynamic analysis of Li ion in multi-walled carbon nanotubes. Mater Chem Phys 99:190–196. doi:10.1016/j.matchemphys.2005.09.035
52. Landi BJ, Ganter MJ, Schauerman CM, Cress CD, Raffaelle RP (2008) Lithium ion capacity of single wall carbon nanotube paper electrodes. J Phys Chem C 112:7509–7515. doi:10.1021/jp710921k
53. Landi BJ, Ganter MJ, Cress CD, DiLeo RA, Raffaelle RP (2009) Carbon nanotubes for lithium ion batteries. Energy Environ Sci 2:638–654. doi:10.1039/B904116H
54. Chew SY, Ng SH, Wang J, Novak P, Krumeich F, Chou SL, Chen J, Liu HK (2009) Flexible free-standing carbon nanotube films for model lithium-ion batteries. Carbon 47:2976–2983. doi:10.1016/j.carbon.2009.06.045
55. Landi BJ, DiLeo RA, Schauerman CM, Cress CD, Ganter MJ, Raffaelle RP (2009) Multi-walled carbon nanotube paper anodes for lithium ion batteries. J Nanosci Nanotechnol 9:3406–3410. doi:10.1166/jnn.2009.NS09
56. Landi BJ, Cress CD, Raffaelle RP (2010) High energy density lithium-ion batteries with carbon nanotube anodes. J Mater Res 25:1636–1644. doi:10.1557/JMR.2010.0209
57. Hu L, Wu H, Mantia FL, Yang Y, Cui Y (2010) Thin, flexible secondary Li-ion paper batteries. ACS Nano 4:5843–5848. doi:10.1021/nn1018158
58. Lahiri I, Oh SW, Hwang JY, Cho S, Sun YK, Banerjee R, Choi W (2010) High capacity and excellent stability of lithium ion battery anode using interface-controlled binder-free multiwall carbon nanotubes grown on copper. ACS Nano 4:3440–3446. doi:10.1021/nn100400r
59. DiLeo RA, Castiglia A, Ganter MJ, Rogers RE, Cress CD, Raffaelle RP, Landi BJ (2010) Enhanced capacity and rate capability of carbon nanotube based anodes with titanium contacts for lithium ion batteries. ACS Nano 4:6121–6131. doi:10.1021/nn1018494
60. Welna DT, Qu L, Taylor BE, Dai L, Durstock MF (2011) Vertically aligned carbon nanotube electrodes for lithium-ion batteries. J Power Sources 196:1455–1460. doi:10.1016/j.jpowsour.2010.08.003
61. Zhang D, Zhao Y, Goodenough JB, Lu Y, Chen C, Wang L, Liu J (2011) Exfoliation from carbon nanotubes versus tube size on lithium insertion. Electrochem Commun 13:125–128. doi:10.1016/j.elecom.2010.11.031
62. Schnorr JM, Swager TM (2011) Emerging applications of carbon nanotubes. Chem Mater 23:646–657. doi:10.1021/cm102406h
63. Sivakkumar SR, Kim DW (2007) Polyaniline/carbon nanotube composite cathode for rechargeable lithium polymer batteries assembled with gel polymer electrolyte. J Electrochem Soc 154:A134–A139. doi:10.1149/1.2404901
64. Lota G, Grzyb B, Machnikowska H, Machnikowski J, Frackowiak E (2005) Effect of nitrogen in carbon electrode on the supercapacitor performance. Chem Phys Lett 404:53–58. doi:10.1016/j.cplett.2005.01.074
65. Kim YJ, Abe Y, Yanagiura T, Park KC, Shimizu M, Iwazaki T, Nakagawa S, Endo M, Dresselhaus MS (2007) Easy preparation of nitrogen-enriched carbon materials from peptides of silk fibroins and their use to produce a high volumetric energy density in supercapacitors. Carbon 45:2116–2125. doi:10.1016/j.carbon.2007.05.026
66. Zhang CX, Duan YL, Xing BL, Zhan L, Qiao WM, Ling LC (2009) Influence of nitrogen hetero-substitution on the electrochemical performance of coal-based activated carbons measured in non-aqueous electrolyte. Min Sci Technol (China) 19:295–299. doi:10.1016/S1674-5264(09)60055-7
67. Yang M, Cheng B, Song H, Chen X (2010) Preparation and electrochemical performance of polyaniline-based carbon nanotubes as electrode material for supercapacitor. Electrochim Acta 55:7021–7027. doi:10.1016/j.electacta.2010.06.077
68. Kawaguchi M, Itoh A, Yagi S, Oda H (2007) Preparation and characterization of carbonaceous materials containing nitrogen as electrochemical capacitor. J Power Sources 172:481–486. doi:10.1016/j.jpowsour.2007.07.023
69. Jurcakova DH, Kodama M, Shiraishi S, Hatori H, Zhu ZH, Lu GQ (2009) Nitrogen-enriched nonporous carbon electrodes with extraordinary supercapacitance. Adv Funct Mater 19:1800–1809. doi:10.1002/adfm.200801100
70. Shin WH, Jeong HM, Kim BG, Kang JK, Choi JW (2012) Nitrogen-doped multiwall carbon nanotubes for lithium storage with extremely high capacity. Nano Lett 12:2283–2288. doi:10.1021/nl3000908